RSC Advances

Novel magnetic core-shell Ce-Ti@Fe3O4 nanoparticles as adsorbent for water contaminants removal

Journal:	*RSC Advances*
Manuscript ID	Draft
Article Type:	Communication
Date Submitted by the Author:	n/a
Complete List of Authors:	Abo Makeb, Ahmad; Universitat Autonoma de Barcelona Ordosgoitia, Laura; Universitat Autonoma de Barcelona Alonso, Amanda; Autonomous University of Barcelona, Chemical, Biological and Environmental Sanchez, Antoni; Universitat Autonoma de Barcelona, Chemical Engineering Department Font, Xavier; Universitat Autonoma de Barcelona, Chemical Engineering Department
Subject area & keyword:	Nanoscience - Environmental < Environmental

Department of Chemical, Biological and Environmental Engineering

University Autonomous of Barcelona (UAB)

08193, Bellaterra, Barcelona, Spain.

10th May 2016

Tel: +34 935814793

e-mail : amanda.alonso@uab.cat

Dear Mike D Ward, Editor-in-chief of RSC Advances Journal,

We are sending the article entitled *Novel magnetic core-shell Ce-Ti@Fe_3O_4 nanoparticles as adsorbent for water contaminants removal* to be considered for publication in *RSC Advances*. This communication is based on one of the topics of most scientific interest nowadays which is the development of new and applicable nanomaterials for environmental applications. In this field, we focused in the development of an improved magnetic core-shell Ce-Ti@Fe_3O_4 nanomaterial which has demonstrated that can be a promising nanomaterial as adsorbent for anionic water contaminants removal, exhibiting high removal capacity for nitrates, phosphates and fluoride compared to others materials reported, what it is also compared in this work. As explained in the communication, the synthesis of nanomaterials and their use for water treatment is also of great interest. It is expected several further publications about the material and its applications from our group. For all of these reasons we guess that this contribution may be considered for publication in *RSC Advances*.

With best wishes,

Dr. Amanda Alonso

Magnetic core-shell Ce-Ti@Fe_3O_4 nanoparticles with high magnetism, crystallinity, stability and adsorption capacity for anionic water contaminants.

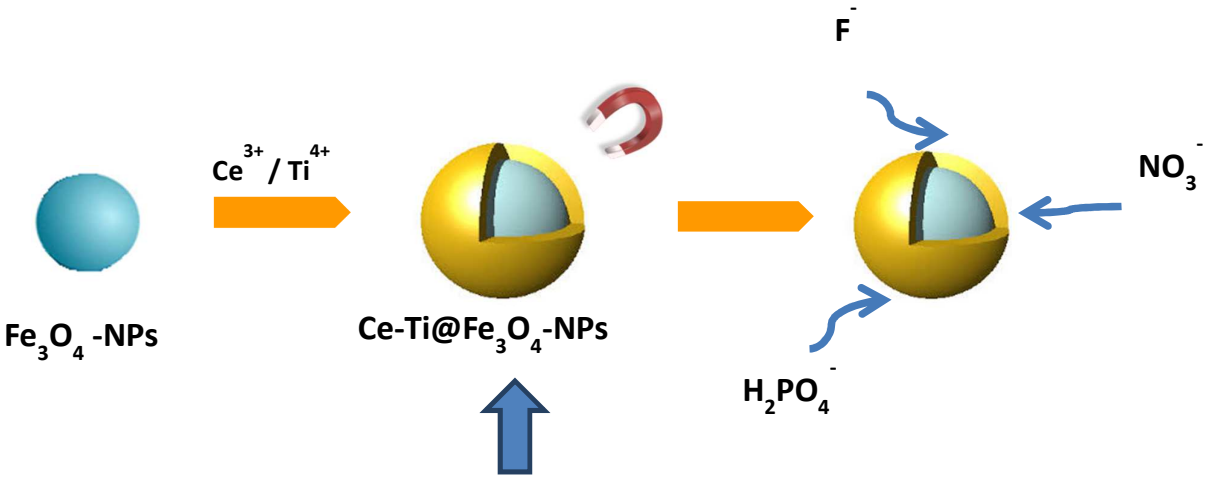

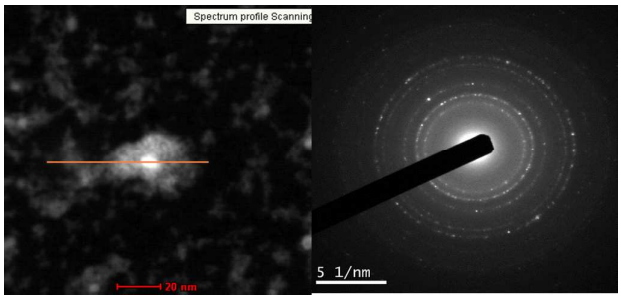

Journal Name

COMMUNICATION

Novel magnetic core-shell Ce-Ti@Fe_3O_4 nanoparticles as adsorbent for water contaminants removal

Received 00th January 20xx,
Accepted 00th January 20xx

DOI: 10.1039/x0xx00000x

www.rsc.org/

Ahmad A. Markeb, Laura A. Ordosgoitia, Amanda Alonso*, Antoni Sánchez, Xavier Font

Magnetic core-shell Ce-Ti@Fe_3O_4 nanoparticles were synthesized by coating cerium titanate on magnetite under mild experimental conditions. Combining magnetism, crystallinity, stability and adsorption capacity, it can be a promising nanomaterial as adsorbent for anionic water contaminants, exhibiting high removal capacity, from 85% to 100%, for nitrates, phosphates and fluoride.

Contamination of water is a widespread problem throughout the world as a result of pollution and a wide range of pollutants can be considered for remediation[1]. Thus, the development of new technologies is fundamental. Among all the current decontamination methods, adsorption is considered the most effective, environmental friendly, and economically method for contaminants removal[2]. In addition, nanotechnology can offer new products and process alternatives for water purification[3]. Some examples are based on nanoparticles (NPs), nanomembranes, carbon nanotubes (CNTs) and nanofibers, among others[4]. Thus, the use of adsorbents nanomaterials has become an interesting way for the removal of various contaminants from drinking water[5] such as of heavy metals[6] and, in a minor extent, nutrients[7]. For instance, the use of CeO_2, Fe_3O_4 and TiO_2 NPs and magnetic nanocomposite[7] for the adsorption of cadmium[8] and phosphate[7,9] has been reported by our group. Finally, other metal oxides and metal hydroxides had also been reported[10] for fluoride removal from water as well as bimetallic or mixed oxides[11]. Further, it is worthy to consider the reusability and the regeneration of the adsorbents as well as the trapping of the NPs to prevent its environmental and health safety risks[12]. Thus, the use of magnetic NPs for pollutants removal provides efficient, easy separation, and reusability. The magnetic NPs can be either used directly or as the core material in a core-shell NPs structure[13]. For instance, cerium titanates nanomaterials ($Ce_{2/3}TiO_3$) have many applications as photocatalytic and ferroelectric materials[14]. However, its properties exhibits canted-antiferromagnetic order[15] and few studies for improving its properties have been reported[16]. In this work, a novel nanomaterial was synthesized by coating cerium titanate on magnetite NPs using a simple and easy method as one step synthesis under room temperature to obtain magnetic core-shell Ce-Ti@Fe_3O_4 NPs (shell@core). Moreover, its efficiency was demonstrated for water remediation as a versatile nanoadsorbent for typical inorganic contaminants.

Briefly, the synthesis of the nanoadsorbent here reported was based in the following procedure: previously of the synthesis of the core-shell Ce-Ti@Fe_3O_4 NPs, magnetite nanoparticles (Fe_3O_4-NPs) were prepared by the co-precipitation method as reported elsewhere[7,17] by using cetyl trimethyl ammonium bromide, CTAB, as dispersant. During the synthesis, the mixture's colour turned from light yellow to red brown and then eventually to black which confirmed the formation of Fe_3O_4-NPs. Once the Fe_3O_4-NPs were washed and dried, Ce-Ti@Fe_3O_4 NPs were synthetized. $TiCl_4$ and $Ce(NO_3)_3{\cdot}6H_2O$ were mixed with 100 mL of Milli-Q water containing the previous formed Fe_3O_4-NPs, with a Ti^{4+}:Ce^{3+} molar ratio of 1:1 and to reach a total molar concentration of 50 mM. Mixing was under agitation at room temperature for 30 min. Next, a slowly dropwise titration with 12.5 %v/v NH_3 solution until pH 7.0 was reached. Then, the Ce-Ti@Fe_3O_4 NPs produced were washed with ultrapure water and magnetic decantation and finally dried at 80 °C for 24h. The synthetic procedure was adapted from similar works about core-shell magnetic Ti-NPs synthesis[13a]. Further details about the materials used and the synthetic protocols are found in *Electronic Supplementary Information* †ESI.1. The Ce-Ti@Fe_3O_4 nanomaterial obtained was fully characterized for a deep understanding of its structure and properties. Thus, the metal content of the Ce-Ti@Fe_3O_4 NPs was determined by *Inductively Coupled Plasma Optical Emission Spectrometry*, ICP–OES (†ESI.2.1). The metal content (Ce, Ti and Fe) is detailed in terms of mg_M/g and $mmol_M/g$ of the nanomaterial, where M corresponds to Ti, Ce and Fe, respectively. The results showed a metal content of 121.01±7.70 mgTi/g, 199.29±10.47 mgCe/g and 81.07±4.49 mgFe/g, meaning 2.50±0.16 mmolTi/g, 1.40±0.07 mmolCe/g and 1.50±0.08 mmolFe/g. Thus, the synthesized nanoadsorbent contents the

Department of Chemical, Biological and Environmental Engineering. Universitat Autònoma de Barcelona. 08193-Bellaterra (Spain)

† Electronic Supplementary Information (ESI) available. See DOI: 10.1039/x0xx00000x

molar ratio of Ce:Ti:Fe of 1:2:1, which is in accordance with the experimental synthetic protocol. *High Resolution Transmission Electron Microscopy* (HRTEM) coupled with *Energy-Dispersive Spectroscopy* (EDS), and *Electron Diffraction* (ED) *Pattern* were used to characterize the morphology, size and crystalline structure of the Ce-Ti@Fe_3O_4 NPs (†ESI.2.2). Fig. 1 illustrates the TEM images coupled with EDS and ED pattern for Ce-Ti@Fe_3O_4 NPs. As shown in Fig.1a, Ce-Ti@Fe_3O_4 NPs present a particle size within the range of 10 – 15 nm. Electron diffraction pattern allows studying the crystal structure of the NPs. Thus, the ED pattern for Ce-Ti@Fe_3O_4 NPs (Fig. 1b), taken from randomly selected area of the nanomaterial (SAED), exhibits multiple rings consisting of discrete spots, which suggested that the core-shell NP is based on nanocrystals.

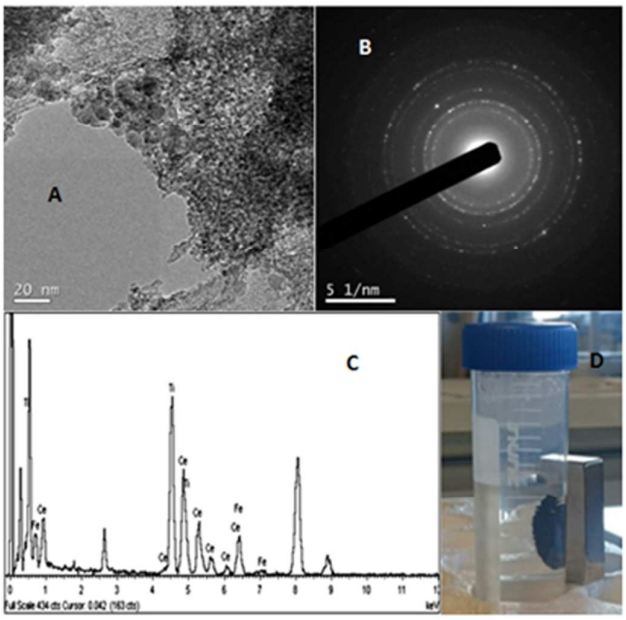

Fig. 1

In addition, EDS provided the metal composition of the samples and Fig. 1c proved the presence of the three components Ce, Ti, and Fe in the material. Moreover, magnetic properties of the Ce-Ti@Fe_3O_4 nanomaterial were qualitatively tested using a square magnet, showing the strong magnetism of the material (Fig. 1d). This result demonstrates an enhancement on its properties comparing to the literature where $Ce_{2/3}TiO_3$ exhibits antiferromagnetic properties[15]. This also demonstrates that the NPs could be easily recovered from the reaction mixture for further reuse in its application. Further, as shown in Table S1 (†ESI.2.2), the calculated interplanar distance (d) from the SAED pattern of the Ce-Ti@Fe_3O_4 NPs and the corresponding Miller indices (h k l diffraction plan) were compared to the standard values[18]. The values concluded that the crystal pattern presented similarity to both cerium titanate and Fe_3O_4 patterns, which was in agreement with the XRD data further reported.

XRD technique was used to obtain the crystalline structure of the Ce-Ti@Fe_3O_4 NPs. In a diffraction pattern, the location of the peaks on the bragg angles (2θ scale) can be compared to the reference peaks (†ESI.2.3). Fig. 2 shows the XRD pattern of the original Ce-Ti@Fe_3O_4 nanomaterial, which consists of two phases: magnetite and cerium titanate reference patterns that were proved by matching from database (Table S.2, †ESI.2.3). Additionally, Table S.3 (†ESI.2.3) shows the experimental 2θ positions from the XRD pattern and its comparison with the standard 2θ values[18] and their respective Diffracting Plan Index (h k l) in Fe_3O_4 and Ce-Ti oxide NPs. These results could suggest that the diffracted peaks can be indexed to be face centre cubic structure of the Fe_3O_4 NPs according to the JCPDS 00-001-111118b. From the XRD patterns shown in Fig. 2, one can notice the characteristic diffraction peaks belonging to cubic Fe_3O_4. They correspond to (220), (311), (400), (511) and (440) family planes (PDF 89–4319). After cerium titanium oxide coating, the characteristic peaks of cerium titanate were appeared and its bragg angles were found to be close to that of $Ce_{2/3}TiO_{2.98}$. Two peaks were observed corresponding to rutile/anatase in the magnetic cerium titanate NPs: (110) peak of anatase and (101) peak of rutile closely positioned at each other, namely at around 2θ = 25.3 and 2θ = 27.4, respectively.

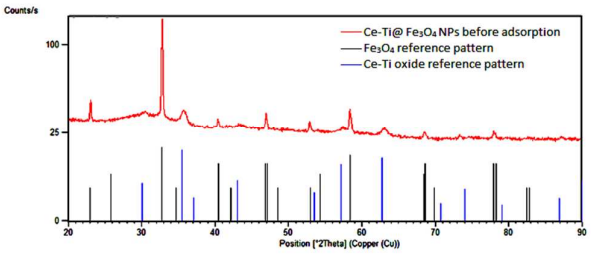

Fig.2

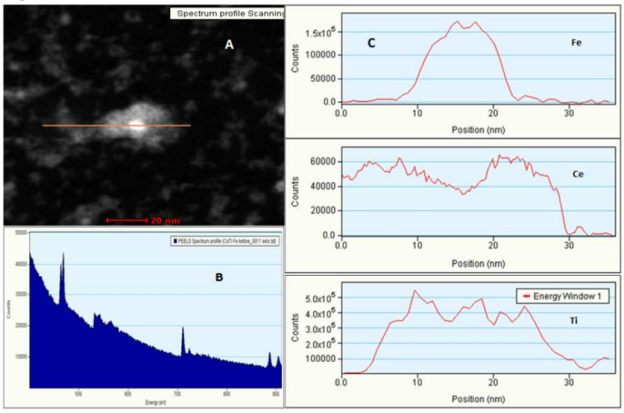

Fig.3

The morphology of the core-shell structure of the Ce-Ti@Fe_3O_4 nanomaterial was demonstrated by *Scanning Transmission Electron Microscopy* (STEM) coupled with *Electron Energy Loss Spectra* (EELS), (†ESI.2.4). Thus, the images obtained from a HAADF detector provide density-based contrast, the cores appearing bright due to their higher scattering probability.[19] As illustrated in Fig. 3, the HAADF image of Ce-Ti@Fe_3O_4 shows that the Fe_3O_4 NPs was coated with Ce-Ti oxide layer (Fig. 3a), moreover STEM based EDS was used to confirm the elemental distribution of the Ti, Fe and Ce, respectively, as shown in Figure 3b. In addition, the scanning line profile appears as a strong peak corresponding to the

position of the bright Fe particle core, whilst the spectra on each side of the core are dominated by Ce and Ti edges as illustrated in Fig.3c.

UV/Vis Absorption and luminescence spectra of Ce-Ti@Fe_3O_4 NPs were performed to estimate the valence of the cerium in the NP and confirm its speciation (†ESI.2.5). As reported, the cerium ion in the cerium titanate, $Ce_{2/3}TiO_3$, is mainly Ce(III).[16] Fig. S.1 (†ESI.2.5) shows the absorption UV-Vis spectra of the Ce-Ti@Fe_3O_4 nanomaterial. As shown, two peaks were observed at 250 and 310 nm respectively, which could be attributed to the presence of either Ce(III) or both Ce(III) and Ce(IV) in the nanomaterial[20]. Therefore, because of the overlapping of both bands, it is difficult to determine the species responsible of colour with the colorimetric technique. Thus, luminescence spectroscopy is necessary to obtain information about the valence of the cerium. Ce(III) ions presents a characteristic intense blue emission upon UV excitation.[21] Therefore, Fig. S.2 (†ESI.2.5) represents the excitation and emission spectra of the Ce-Ti@Fe_3O_4 nanomaterial. The excitation spectrum for λ_{em}=363 nm shows a band at 258 nm and the emission spectrum recorded upon λ_{exc}=266 nm shows the characteristic emission band at 325 nm, which corresponds to the transition to ground state to excited state as compared to literature.[20,22,23] The slightly shift of the wavelength comparing to the literature could be attributed to the lower temperature of the synthesis of the materials andto the presence of magnetite NPs in the core.

In this work, we also investigated the adsorption capacity and removal efficiency of the nanomaterials for different water contaminants: fluoride, nitrate, phosphates and cadmium. The adsorption experiments procedures are based on batch adsorption tests to determine the adsorption efficiency by the synthesized NPs (†ESI.4). Residual contaminant concentration in the solution after 24h of adsorption (Ce) was determined by the corresponding analytical method detailed in †ESI.3 and the equilibrium adsorption capacity (Qe) of the adsorbent was calculated as Equation S.1 (†ESI.4). Adsorption experiments were performed using different initial concentrations for each contaminant that are based either on the reported typical concentration in water or on the maximum contaminated level (MCL). For instance, phosphate initial concentration tested was 10 mg/L due to municipal wastewater may contain 4-15 mg/L, and domestic wastewater may contains 10-30 mg/L[7]. Furthermore, 10 mg/L was selected as initial fluoride concentration because the maximum contaminated level in water is 1.5 mg/L[24]. In the case of fluoride,it has been reported that its concentration in groundwater ranges from well under 1.0 mg/L to more than 35.0 mg/L in several regions.[25] In addition, the initial nitrate concentration tested is 50 mg/L according to the WHO guidelines, where the MCL is 50 mg/L[24b]. Also, 10 mg/L of initial cadmium concentration was selected as wastewater contains 10 – 100 mg/L of cadmium contaminant[26]. All the experiments were performed at pH 7 as a typical value in real media. Table 1 shows the equilibrium adsorption capacities after 24h, the percentage of removal of each contaminant using a concentration of 1g/L of the nanoadsorbent for all the cases.

Table 1

Pollutant	Initial concentration, mg/L	Dose, g/L	Q_e, mg/g	Removal, %
PO_4-P	10	0.90	11.10	99.90
F	10	0.97	10.31	100.0
NO_3-N	50	1.0	42.50	85.00
Cd^{2+}	10	1.0	4.53	45.28

It is shown that the Ce-Ti@Fe_3O_4 NPs have a potential effect for removal anionic contaminants (*i.e.* fluoride, nitrate and phosphates) from 85% removal for nitrate to 100% for phosphates and fluoride. However, it presents low removal for cationic contaminants such as cadmium (45% removal). The differences obtained on the adsorption process for the different contaminants tested may be discussed in terms of the physicochemical properties of the material and thus, the adsorption mechanism of the Ce-Ti@Fe_3O_4 material could be hypothesized. On the one hand, the metal oxides NPs present a relatively negative charge (hydroxyl groups, OH-) on the oxide surface due to its hydrolysis in aqueous media. On the other hand, as discussed in this study, Ce-Ti@Fe_3O_4 NPs consist of Ce(III) ions and also it has a potential of +165 mV at pH 7. Thus, different sorption processes could take place for these contaminants tested. The adsorption mechanism for the anions could be attributed to two explanations: i) electrostatic attraction (i.e. chemisorption)[27] and ii) surface ion-exchange process (i.e. physisorption)[28]. In the first case, phosphate removal could be explained in terms of the formation of cerium phosphate, as reported.[29] In the second case, the OH-groups on the adsorbent surface played a dominant role. Therefore, fluoride or nitrate removal may suffer a surface ion-exchange process based on the exchange of the OH- group with the contaminant anion[28]. Also, electrostatic force could take place between the anions and the positive charge from the quaternary ammonium group from the cross-linker CTAB, used in the synthetic protocol as stabilizer. It has been reported that heavy metal adsorption onto NPs is an emerging technique for the removal of these pollutants due to its suitable electric charge given by an adequate Z-potential[30]. However, Ce-Ti@Fe_3O_4 material shows a low removal for cadmium due to the positive charge of the NPs surface (positive potential) that contributes to a weak electrostatic interaction between cadmium and the OH- from the oxide surface of the NPs. Further, the efficiency of this material was demonstrated by comparing the equilibrium adsorption capacities with those reported in literature (Table SI.2, †ESI.4). As indicated, Ce-Ti@Fe_3O_4 NPs show high efficiency for anions comparing to cations. Thus, further studies on the promising properties of this new material in terms of adsorption capacity should be focused on anionic pollutants dissolved in water.

Conclusions

Magnetic core-shell Ce-Ti@Fe_3O_4 nanoparticles were designed and synthesized by incorporating magnetite into Ce-

Ti oxide nanoparticles by mild experimental conditions. The resulting magnetic and core-shell nanomaterial exhibited a suitable composition, crystallinity and magnetic properties to be functional as nanoadsorbent for the removal of inorganic pollutants from aqueous media. Remarkably, the adsorption capacity and removal efficiency at pH 7 for anionic contaminants such as nitrates, phosphates and fluoride was from 85 to 100% under the experimental conditions. In comparison with other materials reported in literature, this nanoadsorbent is highly competitive, as it has high adsorption capacity and it is easy to recover from the reaction mixture for further reuse due to its magnetic properties.

The author, Ahmad Abo Markeb, appreciated and would like to thank the Ministry of Higher Education of Egypt for the Ph.D external mission grant. Special thanks are given to Servei de Microscopia from Universitat Autònoma de Barcelona and from the Institut Català de Nanociencia i Nanotecnologia.

Notes and references

1 P. B. Tchounwou, C. G. Yedjou, A. K. Patlolla and D. J. Sutton, in Molecular, Clinical and Environmental Toxicology: Volume 3: Environmental Toxicology, ed. A. Luch, Springer Basel, Basel, 2012, 133.

2 A. Bhatnagar, E. Kumar and M. Sillanpää, Chemical Engineering Journal, 2011, 171, 811.

3 I. Gehrke, A. Geiser and A. Somborn-Schulz, Nanotechnology, Science and Applications, 2015, 8, 1.

4 S. Recillas, J. Colón, E. Casals, E. González, V. Puntes, A. Sánchez and X. Font, Journal of Hazardous Materials, 2010, 184, 425.

5 X. Qu, P. J. J. Alvarez and Q. Li, Water Research, 2013, 47, 3931.

6 A. Sánchez, S. Recillas, X. Font, E. Casals, E. González and V. Puntes, TrAC Trends in Analytical Chemistry, 2011, 30, 507.

7 A. Abo Markeb, A. Alonso, A. D. Dorado, A. Sánchez and X. Font, Environmental Technology, 2016, 1.

8 A. R. Contreras, A. García, E. González, E. Casals, V. Puntes, A. Sánchez, X. Font and S. Recillas, Desalination and Water Treatment, 2012, 41, 296.

9 S. Recillas, A. García, E. González, E. Casals, V. Puntes, A. Sánchez and X. Font, Water Science and Technology, 2012, 66, 503.

10 (a) E. Kumar, A. Bhatnagar, U. Kumar and M. Sillanpää, Journal of Hazardous Materials, 2011, 186, 1042; (b) G. Lee, C. Chen, S.-T. Yang and W.-S. Ahn, Microporous and Mesoporous Materials, 2010, 127, 152; (c) S.-X. Teng, S.-G. Wang, W.-X. Gong, X.-W. Liu and B.-Y. Gao, Journal of Hazardous Materials, 2009, 168, 1004; (d) S.M. Maliyekkal, A. K. Sharma and L. Philip, Water Research, 2006, 40, 3497; (e) S. S. Tripathy, J.-L. Bersillon and K. Gopal, Separation and Purification Technology, 2006, 50, 310; (f) S. Ghorai and K. K. Pant, Separation and Purification Technology, 2005, 42, 265; (g) K. Biswas, D. Bandhoyapadhyay and U. C. Ghosh, Adsorption, 2007, 13, 83; (h) K. Biswas, K. Gupta and U. C. Ghosh, Chemical Engineering Journal, 2009, 149, 196; (i) D. Thakre, S. Rayalu, R. Kawade, S. Meshram, J. Subrt and N. Labhsetwar, Journal of Hazardous Materials, 2010, 180, 122; (j) N. Minju, K. Venkat Swaroop, K. Haribabu, V. Sivasubramanian and P. Senthil Kumar, Desalination and Water Treatment, 2013, 53, 2905; (k) V.Sivasankar, T. Ramachandramoorthy and A. Darchen, Desalination, 2011, 272, 179.

11 (a) V. Tomar, S. Prasad and D. Kumar, Microchemical Journal, 2013, 111, 116; (b) S. Deng, H. Liu, W. Zhou, J. Huang and G. Yu, Journal of Hazardous Materials, 2011, 186, 1360; (c) L. Chen, T.-J. Wang, H.-X. Wu, Y. Jin, Y. Zhang and X.-M. Dou, Powder Technology, 2011, 206, 291; (d) H.-X. Wu, T.-J. Wang, L. Chen, Y. Jin, Y. Zhang and X.-M. Dou, Powder Technology, 2011, 209, 92; (e) M. G. Sujana and S. Anand, Applied Surface Science, 2010, 256, 6956; (f) X. Wu, Y. Zhang, X. Dou and M. Yang, Chemosphere, 2007, 69, 1758; (g) N. Chen, Z. Zhang, C. Feng, M. Li, D. Zhu and N. Sugiura, Materials Chemistry and Physics, 2011, 125, 293; (h) N. Chen, Z. Zhang, C. Feng, N. Sugiura, M. Li and R. Chen, Journal of Colloid and Interface Science, 2010, 348, 579; (i) H. Liu, S. Deng, Z. Li, G. Yu and J. Huang, Journal of Hazardous Materials, 2010, 179, 424.

12 A. Alonso (2012). Development of polymeric nanocomposites with enhanced distribution of catalytically active or bactericide nanoparticles. Chemistry Departament, Universitat Autònoma de Barcelona, Spain.

13 (a) C. Zhang, L. Chen, T.-J. Wang, C.-L. Su and Y. Jin, Applied Surface Science, 2014, 317, 552; (b) L. Chen, B.-Y. He, S. He, T.-J. Wang, C.-L. Su and Y. Jin, Powder Technology, 2012, 227, 3.

14 L. Kong, D. J. Gregg, I. Karatchevtseva, Z. Zhang, M. G. Blackford, S. C. Middleburgh, G. R. Lumpkin and G. Triani, Inorganic Chemistry, 2014, 53, 6761.

15 K. Yoshii and H. Abe, Journal of Alloys and Compounds, 2002, 343, 199.

16 W. H. Jung, J. Phys.: Condens. Matter, 1998, 10, 8553.

17 S. Laurent, D. Forge, M. Port, A. Roch, C. Robic, L. Vander Elst and R. N. Muller, Chemical Reviews, 2008, 108, 2064.

18 (a) L. G. Berry and R. M. Thompson, Waverly Press: New York, 1962, 194; (b) J. L. Zhang, R. S. Srivastava and R. D. K. Misra, Langmuir, 2007, 23, 6342.

19 B. R. Knappett, P. Abdulkin, E. Ringe, D. A. Jefferson, S. Lozano-Perez, T. C. Rojas, A. Fernandez and A. E. H. Wheatley, Nanoscale, 2013, 5, 5765.

20 M. Martos, B. Julián-López, J. V. Folgado, E. Cordoncillo and P. Escribano, European Journal of Inorganic Chemistry, 2008, 2008, 3163.

21 L. Huang, X. Wang, H. Lin and X. Liu, Journal of Alloys and Compounds, 2001, 316, 256.

22 G. Q. Xu, Z. X. Zheng, W. M. Tang and Y. C. Wu, Journal of Luminescence, 2007, 124, 151.

23 E. Cordoncillo, F. J. Guaita, P. Escribano, C. Philippe, B. Viana and C. Sanchez, Optical Materials, 2001, 18, 309.

24 (a) WHO, 2006, 1 third edition, Geneva, 375; (b) p. i. Drinking-water, WHO, 2004.

25 Meenakshi and R. C. Maheshwari, Journal of Hazardous Materials, 2006, 137, 456.

26 Y. Yurekli, Journal of Hazardous Materials, 2016, 309, 53.

27 M. Pattanaik and S. K. Bhaumik, Materials Letters, 2000, 44, 352.

28 K. Zhang, S. Wu, X. Wang, J. He, B. Sun, Y. Jia, T. Luo, F. Meng, Z. Jin, D. Lin, W. Shen, L. Kong and J. Liu, Journal of Colloid and Interface Science, 2015, 446, 194.

29 Y. G. Ko, T. Do, Y. Chun, C. H. Kim, U. S. Choi and J.-Y. Kim, Journal of Hazardous Materials, 2016, 307, 91.

30 A. R. C. Rodríguez, in Departament d'Enginyeria Química Universitat Autònoma de Barcelona (UAB), Escola d'Enginyeria, 2015.

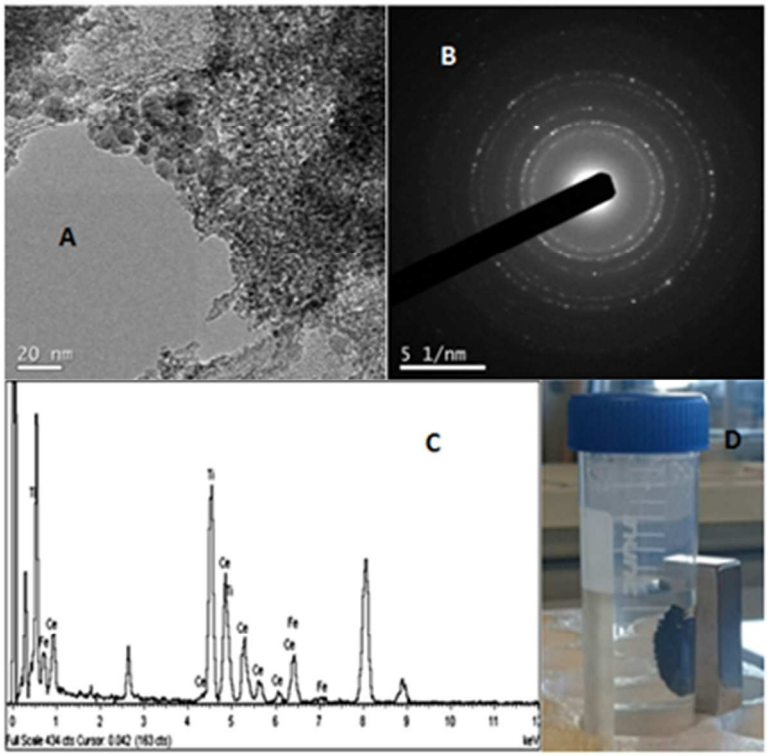

Fig.1. (a) HRTEM image, (b) SAED pattern; (c) EDS spectra and; (d) qualitative magnetic properties test for Ce-Ti@Fe_3O_4 NPs.

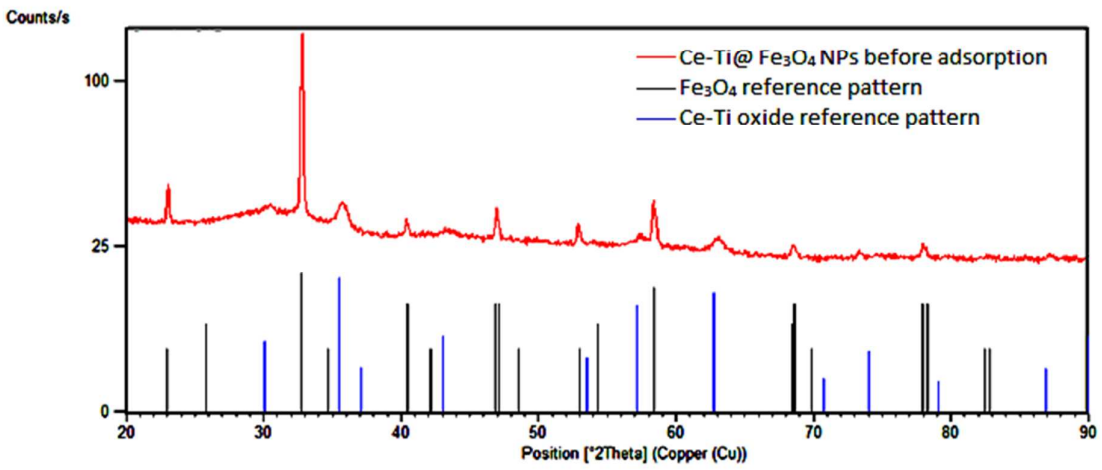

Fig. 2. XRD pattern of the Ce-Ti@Fe_3O_4 material and matching comparison with both Fe_3O_4 and Ce-Ti oxide reference pattern from database.

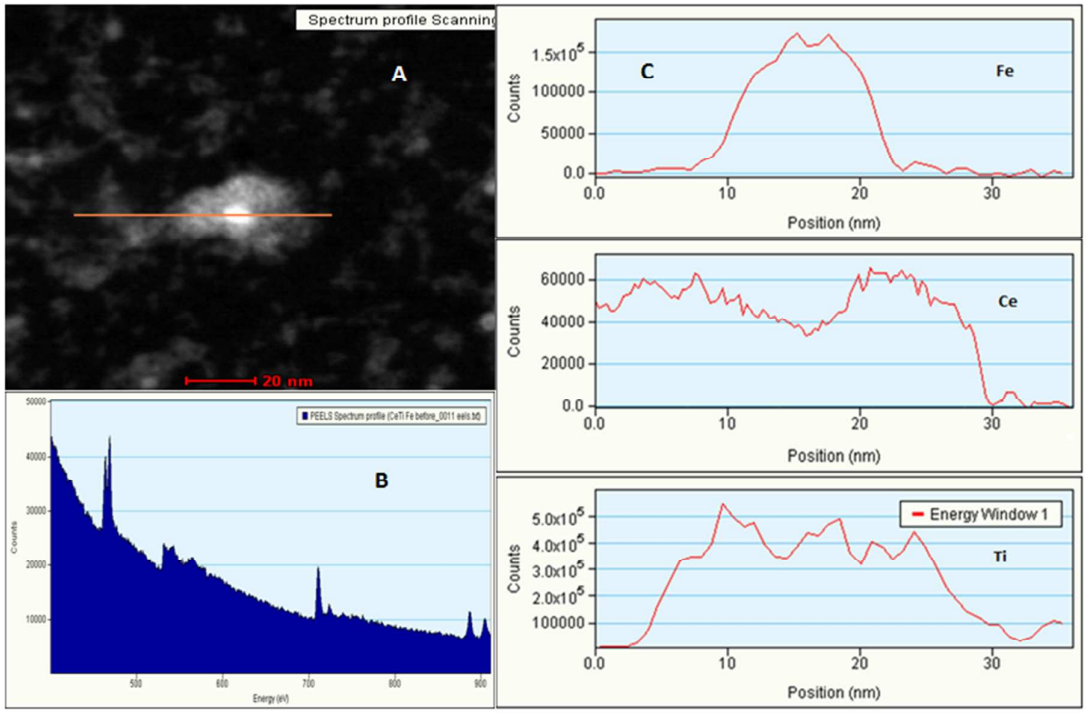

Fig. 3. EELS line scan of the core-shell Ce-Ti@Fe_3O_4 nanocomposite. (A) STEM HAADF image of the Ce-Ti@Fe_3O_4 and position of line scan; (B) PEELS spectrum of the nanocomposite; and (C) Ions profile spectra along the line scaninng.

Table 1 Adsorption capacities and removal efficiencies values for contaminants removal

Pollutant	Initial concentration, mg/L	Dose, g/L	Q_e, mg/g	Removal, %
PO_4-P	10	0.90	11.10	99.90
F	10	0.97	10.31	100.0
NO_3-N	50	1.0	42.50	85.00
Cd^{2+}	10	1.0	4.53	45.28

Electronic Supplementary Information

Novel magnetic core-shell Ce-Ti@Fe_3O_4 nanoparticles as adsorbent for water contaminants removal

Ahmad A. Markeb, Laura A. Ordosgoitia, Amanda Alonso*, Antoni Sánchez, Xavier Font

ESI.1. Materials and Methods

ESI.1.1. Materials

Iron (II) chloride ($FeCl_2$), iron (III) chloride hexahydrate ($FeCl_3 \cdot 6H_2O$), sodium fluoride (NaF), titanium chloride ($TiCl_4$), cerium nitrate hexahydrate ($Ce(NO_3)_3 \cdot 6H_2O$), ammonia (NH_3) solution, and cetyltrimethyl ammonium bromide (CTAB), sodium phosphate monobasic; NaH_2PO_4, cadmium chloride ($CdCl_2$), dithizone, chloroform ($CHCl_3$), potassium cyanide (KCN), hydroxylamine hydrochloride ($NH_2Cl \cdot H_2O$) were purchased from Sigma-Aldrich, Spain. Sodium hydroxide pellets (NaOH) was purchased from Merk. Hydrochloric acid (HCl), nitric acid (HNO_3) was purchased from Panreac, SA. All the chemicals were of analytical grade or higher, and all solutions were prepared with Milli-Q water and filtered using 0.45 µm Nylon membrane filter.

ESI.1.2. Preparation magnetic Fe_3O_4 nanoparticles

Previously of Ce-Ti@Fe_3O_4 NPs (section 2.2.2), magnetite nanoparticles (Fe_3O_4-NPs) were prepared by the co-precipitation method reported elsewhere. [1] First, $FeCl_2$ and $FeCl_3 \cdot 6H_2O$, with Fe^{2+}/Fe^{3+} molar ratio of 1:2, were dissolved in 100 mL of deoxygenated ultrapure water (Milli-Q) containing 0.1% of CTAB as dispersant.

Then, the suspension was incubated for 1 hour at 40 °C and under N_2 atmosphere. Secondly, 0.6 M NH_3 solution was titrated into the iron salts solution under agitation until the pH 9.0 achieved. During titration process, the mixture's color turned from light yellow to red brown and then eventually to black which confirmed the formation of Fe_3O_4-NPs. Then, the suspension containing Fe_3O_4-NPs incubated for 1 hour under N_2 and at 40 °C. Afterwards, the NPs were washed three times using ultrapure water and magnetic decantation.

ESI.2. Characterization of the Ce-Ti@Fe_3O_4 NPs

ESI.2.1. Inductively Coupled Plasma Optical Emission Spectrometry (ICP-OES)

ICP-OES was used for the metal concentration analysis in the synthesized nanoadsorbent. Fe, Ce and Ti metals from the nanoparticles were analyzed by using ICP-OES, Perkin Elmer model Optima 4300DV. The pre-treatment of the samples consists of an acid digestion of the nanoadsorbent, dilution with MilliQ-water and filtration using 0.45 μm Nylon filters. The metal amounts are reported in terms of mg_M/g (mg of metal per mass of the nanoadsorbent) and $mmol_M/g$ (mmol of metal per mass of the nanoadsorbent). All measures were performed in triplicate. The Relative Standard Deviation (RSD) for all the measurements is 2%. Analyses were performed at Servei d'Anàlisi Química, Universitat Autònoma de Barcelona (UAB), Spain.

ESI.2.2. High Resolution Transmission Electron Microscopy (HRTEM) coupled with Energy-Dispersive Spectroscopy (EDS), and Electron Diffraction (ED) Pattern.

JEM-2011/JEOL microscope from Servei de Microscopia at UAB used to characterize the morphology and sizes of the NPs. The samples were dispersed with

ethanol and deposited on a Cu grid [2]. EDS provided the metal chemical composition of the samples based on the X-Rays emitted by an atom that has been interacted with an electron beam. Measurements were acquired with an Oxford INCA X-MAX detector [3]. Electron diffraction pattern allows studying the crystal structure of the NPs. The periodic structure of a crystalline solid acts as a diffraction grating, scattering the electrons in a predictable manner. Working back from the observed diffraction pattern, it may be possible to deduce the structure of the crystal producing the diffraction pattern [4]. Electron diffraction is also a useful technique to study the short range order of amorphous solids.

Table S1. Comparison of experimental and standard Interplanar Spacing (d) values with their respective Diffracting Plan Index (h k l) in Fe_3O_4 and Ce-Ti oxide Nanoparticles using ED pattern.

d, °A experimental	Fe_3O_4 NPs		Ce-Ti oxide NPs	
	d, °A standard	hkl	d, °A standard	hkl
3.01	2.97	220	---	---
2.74	---	---	2.73	110
2.47	2.53	311	---	---
2.20	---	---	2.23	112
2.06	2.10	400	---	---
2.04	---	---	1.94	004
1.86	---	---	1.87	201
1.77	---	---	1.73	210
1.68	---	---	1.69	211
1.56	---	---	1.58	212
1.42	1.48	440	---	---

ESI.2.3. X-Ray Diffraction (XRD)

XRD technique was used to obtain the crystalline structure of the Ce-Ti@Fe_3O_4 NPs. In a diffraction pattern, the location of the peaks on the bragg angles (2θ scale) can be compared to reference peaks. The identification of magnetite and cerium titanate were based on the characteristic peaks in the diffractograms and comparing with the database

(*Table S2*) [4-5]. Diffraction patterns were collected on Panalytical X´Pert PRO MPD (Multipurpose Diffractometer). Analyses were performed at Institut Català de Nanociència i Nanotecnologia (ICN2), Spain.

Table S.2. XRD Database reference patterns

Reference code:	00-033-0342	**Reference code:**	00-001-1111
PDF index name:	Cerium Titanium Oxide	**Mineral name:**	Magnetite
Empirical formula:	Ce0.66O2.98Ti	**Empirical formula:**	Fe3O4
Chemical formula:	Ce0.66TiO2.975	**Chemical formula:**	Fe3O4
		PDF index name:	Iron Oxide

Table S.3 Comparison of experimental and standard (2θ) values with their respective Diffracting Plan Index (h k l) in Fe_3O_4 and Ce-Ti oxide NPs using XRD pattern

2θ experimental	**Fe_3O_4 NPs**		**Ce-Ti oxide NPs**	
	2θ standard	**hkl Diffraction plan**	**2θ standard**	**hkl Diffraction plan**
23.13	---	---	25.82	101
31.42	30.06	220	---	---
32.85	---	---	32.74	110
35.77	35.45	311	---	---
40.44	---	---	40.45	112
43.64	43.04	400	---	---
47.14	---	---	46.82	004
52.98	---	---	52.98	210
57.45	57.17	511	---	---
58.42	---	---	58.44	212
63.18	62.73	440	---	---
68.63	---	---	68.40	024
78.05	---	---	77.90	106
87.29	86.91	642	---	---
90.20	89.93	731	---	---

ESI.2.4. Scanning Transmission Electron Microscopy (STEM) coupled with Electron Energy Loss Spectra (EELS)

The morphology of the core-shell nanocomposite was estimated by STEM coupled with HAADF detector and EELS. Images were acquired using an FEI Tecnai G2 F20 microscope operated at 200 kV and equipped with a GIF Quantum energy filter. All spectra were recorded using a convergence semiangle of about 12 mrad and a collection semiangle of about 40 mrad. EDX spectra were obtained using an EDAX super ultra-thin window (SUTW) X-ray detector. The sample was first dispersed in ethanol and sonicated, then deposited onto the copper microscopy grid coated with an amorphous carbon film. By imaging with the electrons that have an energy loss corresponding to core losses of particular elements using STEM, one can obtain elemental information with high spatial resolution. A full energy loss spectrum from a series of points across the particle in a STEM configuration, which allows the extraction of linear compositional variation was used to obtain chemical information about the nanostructure. Analyses were performed at Institut Català de Nanociència i Nanotecnologia (ICN2), Spain.

ESI.2.5. UV/VIS and luminescence spectra analysis

Absorption and luminescence spectra of Ce-Ti@Fe_3O_4 NPs were performed to estimate the valency of the cerium in the NP and confirm its speciation. Absorption and luminescence spectra were analyzed using UV/Vis spectrophotometer, Cary 50 bio Varian, and Luminescence spectrometer, LS 55 Perkin Elmer. pH was adjusted using Crison pH meter 2001. Samples are prepared by suspension of 1 g of the core-

shell nanomaterial in 1 L Milli-Q water adjusted to pH 7.0 using 0.1M NaOH.

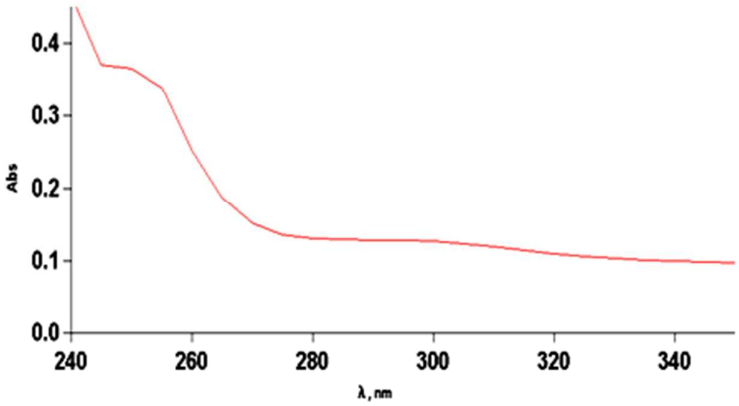

Figure S.1. UV/Vis spectra for Ce-Ti@Fe_3O_4 nanomaterial.

Although the main absorption band is around 310 nm for Ce(III), characteristic broad bands in the UV region between 330 and 200 nm could be observed due to the coexistence of Ce(III) and Ce(IV) species because of its particular electronic configuration. [6]

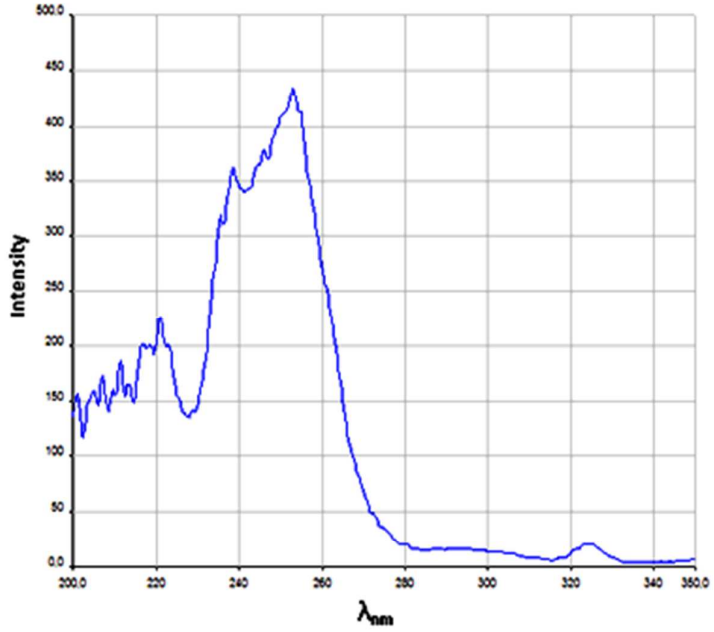

Figure S.2. Luminescence spectra of the Ce-Ti@Fe_3O_4 nanomaterial at the excitation spectrum for λ_{em}=363 nm and the emission spectrum recorded upon λ_{exc}=266 nm.

ESI.3. Analytical methods used in the Adsorption Experiments

ESI.3.1. Ionic chromatography (IC) for fluoride, nitrate and phosphate analysis

The determination of phosphate, as phosphorous (PO_4-P), Fluoride anion (F^-) and nitrate (NO_3-N) was determined using ICS-2000 (Dionex) ion chromatographic system, with ultimate 3000 autosampler. An ion exchange column specifically designed for rapid analysis of inorganic anion (Dionex IonPac AS18, 4 x 250 mm) equipped with an IonPac guard column (Dionex IonPac AG18, 4 x 50 mm) was used. Chromeleon® software was used to acquire data and control the instrumentation. Standard error in the measurements is < 0.1%.

A stock solution of each contaminant was prepared by dissolving the appropriate amount of its precursor in ultrapure water. All working contaminants solutions for calibration curve and adsorption studies were prepared by diluting the stock solution. Calibration standards and samples were filtered using 0.45 μm Nylon membrane filter before injection.

ESI.3.2. UV-Vis for Cadmium analysis

Calibration curves for cadmium were constructed using 99.995% cadmium(II) chloride by using a colorimetric method, based on the reaction of cadmium with dithizone to form a complex that is extracted with chloroform. Then the absorbance is measured at 518nm [7]. Cadmium stock solution was prepared by dissolving the appropriate amount in 5 % nitric acid. The cadmium solutions for calibration curve and adsorption studies were prepared by diluting the stock solution.

ESI.4. Adsorption experiments procedure

Batch adsorption tests were used to determine the adsorption efficiency by the synthesized NPs. A contaminant solution with an initial concentration (C_0) (mg/L) was prepared as mentioned before (section 2.4.1). A concentration of adsorbent (W) (g/L) was added into a conical flask containing 25 mL of the aqueous contaminated solution. pH of the solution was adjusted when necessary using 0.1 M NaOH and/or HCl until pH 7. The flask was shaken (200 rpm) at 25 °C using a thermostat shaker. Residual contaminant concentration in the solution after 24h of adsorption, C_e, was determined by the corresponding analytical method detailed in Section 2.4. Equilibrium adsorption capacity, Q_e, of the adsorbent was calculated as Equation S.1:

$$Q_e = (C_0 - C_e)/\mathrm{W} \quad (1)$$

Adsorption experiments were preformed using different initial concentrations for each contaminant where based on the reported typical concentration in water or on the maximum contaminated level (MCL). For instance, phosphate initial concentration tested was 10 mg/L due to municipal wastewater may contain 4-15 mg/L, and domestic wastewater may contains 10-30 mg/L [1a]. Furthermore, 10 mg/L initial fluoride concentration was selected due the maximum contaminated level in water is 1.5 mg/L [8] but, it has been reported that the fluoride concentrations in groundwater range from well under 1.0 mg/L to more than 35.0 mg/L in several regions of India.[9] In addition, the initial nitrate concentration tested is 50 mg/L due to according WHO guidline the MCL is 50 mg/L [8b]. Also, 10 mg/L intial cadmium coencentration was selected due to wastewater contains 10 – 100 mg/L of cadmium contaminant [10]. All the experiments were performed at pH 7 as a typical value in real media.

Table S.2 Adsorption capacities and removal efficiencies values for contaminants removal from the literature

Pollutant	Nanoadsrbents	Initial concentration, mg/L	Dose, g/L	Q_e, mg/g	Removal, %	Ref.
PO_4-P	Ce-Ti@Fe_3O_4	10	0.90	**11.10**	**99.90**	This work
	C100@Fe_3O_4	10	1.0	3.60	36.00	[1a]
	$Al(OH)_3$	10	2.32	2.46	57.07	[11]
	Fe_3O_4	10	10.0	0.88	88.00	[12]
F	Ce-Ti@Fe_3O_4	10	0.97	**10.31**	**100.0**	This work
	$Al(OH)_3$	10	1.60	5.74	91.84	[13]
NO_3-N	Ce-Ti@Fe_3O_4	50	1.0	**42.50**	**85.00**	This work
	Rice straw activated carbon	50	1.0	9.00	18.00	[14]
Cd^{2+}	Ce-Ti@Fe_3O_4	10	1.0	4.53	45.28	This work
	Cork biomass powder	10	1.0	6.40	64.48	[15]

References

1(a) A. Abo Markeb, A. Alonso, A. D. Dorado, A. Sánchez and X. Font, *Environmental Technology*, 2016, 1; (b) S. Laurent, D. Forge, M. Port, A. Roch, C. Robic, L. Vander Elst and R. N. Muller, *Chemical Reviews*, 2008, **108**, 2064.

2 A. Alonso, N. Vigues, X. Munoz-Berbel, J. Macanas, M. Munoz, J. Mas and D. N. Muraviev, *Chemical Communications*, 2011, **47**, 10464.

3 A. Alonso, A. Shafir, J. Macanás, A. Vallribera, M. Muñoz and D. N. Muraviev, *Catalysis Today*, 2012, **193**, 200.

4 L. G. Berry and R. M. Thompson, *Waverly Press: New York*, 1962, 194.

5 J. L. Zhang, R. S. Srivastava and R. D. K. Misra, *Langmuir*, 2007, **23**, 6342.

6 K. Annapurna, R. N. Dwivedi, P. Kundu and S. Buddhudu, *Materials Letters*, 2004, **58**, 787.

7(a) A. R. Contreras, A. García, E. González, E. Casals, V. Puntes, A. Sánchez, X. Font and S. Recillas, *Desalination and Water Treatment*, 2012, **41**, 296; (b) G. A, C. J and J. D, *American Public Health, Association, American Water Works, Association, Water Environment Federation*, 2005, **21st edition**.

8(a) WHO, 2006, **1 third edition, Geneva**, 375; (b) p. i. Drinking-water, *WHO*, 2004.

9 Meenakshi and R. C. Maheshwari, *Journal of Hazardous Materials*, 2006, **137**, 456.

10 Y. Yurekli, *Journal of Hazardous Materials*, 2016, **309**, 53.

11 P. H. Hsu and D. A. Rennie, *Canadian Journal of Soil Science*, 1962, **42**, 197.

12 G. T. T. Le and P. Sreearunothai, *4th International Conference on Informatics, Environment, Energy and Applications (IPCBEE)*, 2015, **82**.

13 B. Shimelis, F. Zewge and B. S. Chandravanshi, *Bull. Chem. Soc. Ethiop.*, 2006, **20**, 17.

14 S. M. Yakout and A. A. Mostafa, *Journal of Animal and Veterinary Advances*, 2014, **13**, 728.

15 F. Krika, N. Azzouz and M. C. Ncibi, *Arabian Journal of Chemistry*.